MATHEMATICAL METHODS IN THE APPLIED SCIENCES
Math. Meth. Appl. Sci. 2002; **25**:21–48 (DOI: 10.1002/mma.278)
MOS subject classification: 74 K 20; 65 N 25

Eigen-frequencies in thin elastic 3-D domains and Reissner–Mindlin plate models

Monique Dauge[1] and Zohar Yosibash[2,*]

[1] *Institut Mathématique, UMR 6625 du CNRS, Université de Rennes 1, Campus de Beaulieu, 35042 Rennes, France*
[2] *Pearlstone Center for Aeronautical Engineering Studies, Mechanical Engineering Department, Ben-Gurion University of the Negev, Beer-Sheva, Israel*

Communicated by W. Wendland

SUMMARY

The eigen-frequencies of elastic three-dimensional thin plates are addressed and compared to the eigen-frequencies of two-dimensional Reissner–Mindlin plate models obtained by dimension reduction. The qualitative mathematical analysis is supported by quantitative numerical data obtained by the *p*-version finite element method.

The mathematical analysis establishes an asymptotic expansion for the eigen-frequencies in power series of the thickness parameter. Such results are new for orthotropic materials and for the Reissner–Mindlin model. The 3-D and R–M asymptotics have a common first term but differ in their second terms.

Numerical experiments for clamped plates show that for isotropic materials and relatively thin plates the Reissner–Mindlin eigen-frequencies provide a good approximation to the three-dimensional eigen-frequencies. However, for some anisotropic materials this is no longer the case, and relative errors of the order of 30 per cent are obtained even for relatively thin plates. Moreover, we showed that no shear correction factor is known to be optimal in the sense that it provides the best approximation of the R–M eigen-frequencies to their 3-D counterparts uniformly (for all relevant thicknesses range).

KEY WORDS: plates; eigenvalue problems

1. INTRODUCTION

The accurate computation of eigen-frequencies of elastic domains, is of high engineering importance because the smallest frequencies have to be higher compared with any frequency of a dynamically applied load. Otherwise resonance may occur, resulting in the amplification of the eigen-mode and finally the destruction of the elastic structure.

This is of particular importance in three-dimensional thin domains, such as three-dimensional plates, where the smallest eigen-frequencies are proportional to the thickness. It has been

*Correspondence to: Zohar Yosibash, Pearlstone Center for Aeronautical Engineering Studies, Mechanical Engineering Department, Ben-Gurion University of the Negev, Beer-Sheva, Israel

 Received 17 April 2001

shown in References [1, 2] that for isotropic thin plates, the smallest frequencies are associated with bending modes. Therefore, we address herein these bending eigen-frequencies in a fully three-dimensional domain.

Due to the complexity of a three-dimensional eigen-analysis, much attention has been given historically to the derivation of plate models, which can be understood as an application of dimensional reduction principles. These plate models are aimed to approximately solve the three-dimensional *bending* eigen-problem by a two-dimensional formulation. In engineering practice the Reissner–Mindlin (R–M) plate model is frequently used as an approximation of the 3-D thin plate domain, and is assumed to be valid for thicknesses of plates under 5% compared with other dimensions.

In this paper, our aim is a twofold investigation of the quality of approximation of 3-D eigen-frequencies by R–M eigen-frequencies:

1. By a theoretical asymptotic analysis, we obtain after [2, 3] a power series expansion in the thickness parameter ε of both 3-D eigen-frequencies and R–M eigen-frequencies.
2. By a numerical implementation, we quantify the deviation from R–M with respect to 3-D, in a variety of situations for small but non-zero ε's.

The outcome of point 1. is that the 3-D and R–M eigen-frequency asymptotics have *the same first terms* as $\varepsilon \to 0$, namely ε times the corresponding eigen-frequency λ_1 of the limit Kirchhoff–Love model (K–L). But *the second terms* in the asymptotics, as far as lateral clamped boundary conditions are considered, are *always different*: indeed we prove in this paper that this second term for the 3-D eigen-frequency has the form ε^2 times a positive quantity λ_2, whereas for the R–M model, the term in ε^2 is zero.

Thus, from a strictly mathematical point of view, the R–M approximation is not better than the K–L approximation, and in both the cases, this is an order 1 approximation. From a practical point of view, the order of magnitude of the quantity λ_2 with respect to λ_1 is of importance, since the relative error of approximating a 3-D plate by the R–M model is equivalent to $\varepsilon\lambda_2/\lambda_1$ as ε approaches zero, but is still non-zero.

The quantity λ_2 is a coupling term between inner (boundary layer) and outer (regular) parts of a two-scale expansion of eigen-vectors. Moreover, in λ_2 there is a multiplicative factor c^{b} which depends only on the material law of the 3-D plates. For example, for isotropic materials, we show that this factor is an increasing function of the Poisson coefficient ν. For special non-isotropic materials, we show that this factor is much larger.

That is why we extend the results of References [2, 3] to orthotropic materials. The multiplicative factor appears now as a density along the lateral boundary. We also present the corresponding construction of R–M model, and the asymptotics of eigen-frequencies. What is known about asymptotics for the R–M model is References [4, 5] where it is proved that in the loading case, there is no boundary layer at order 1, but that it starts at order 2. This is exactly the reason for the absence of the term of order ε^2 in the eigen-frequency asymptotics.

Numerical experiments with clamped plates are provided. These results quantify the influence of the material law and the shape of the mid-surface on the R–M eigen-frequencies as compared to their 3-D counterparts. It is shown that for isotropic materials and relatively thin plates, the difference is very small, whereas for orthotropic materials the difference in the first eigen-frequency of the R–M plate model and the corresponding eigen-frequency of the fully 3-D plate can be as large as 30%. Moreover, we showed that no shear correction

factor is known to be optimal in the sense that it provides the best approximation of the R–M eigen-frequencies to their 3-D counterparts uniformly (for all thicknesses range).

In Section 2 we provide the mathematical description of the plate models (3-D and R–M model), and in particular summarize the asymptotic behaviour of the eigen-frequencies (in terms of ε). Details about the mathematical analysis on the derivation of the asymptotics of the eigen-frequencies for orthotropic 3-D plates is given in Appendix A and for orthotropic R–M model in Appendix B. The model problems used in the numerical experimentation are described in Section 3, followed by the numerical results in Section 4. Summary and conclusions are given in Section 5.

2. 3-D PLATE VIS REISSNER–MINDLIN PLATE MODEL

2.1. Eigen-frequencies of the 3-D plate

Consider a thin elastic domain Ω of thickness 2ε as shown in Figure 1, defined as follows:

$$\Omega = \omega \times (-\varepsilon, +\varepsilon), \quad \text{with } \omega \subset \mathbb{R}^2 \text{ a regular domain}$$

The co-ordinates are $\mathbf{x} = (x_1, x_2, x_3)$ and the mid-surface ω lies in the plate x_1–x_2, while x_3 is in the normal direction. As a representative case we restrict our attention to clamped boundary conditions on the lateral edges. More precisely, we assume that the upper and lower surfaces of the plate, i.e. $\omega \times \{\pm\varepsilon\}$, are traction free, and that the lateral edges of the plate $\partial\omega \times (-\varepsilon, \varepsilon)$ are clamped, i.e. $\mathbf{u} = \mathbf{0}$. Here $\mathbf{u} = (u_1(\mathbf{x}), u_2(\mathbf{x}), u_3(\mathbf{x}))^{\mathrm{T}}$, denotes the displacement field.

We denote by $\mathbf{e}$ the *engineering notation* of the linear strain tensor. Accordingly, we use the index notation: $(e_1, e_2, e_3, e_4, e_5, e_6) = (e_{11}, e_{22}, e_{33}, 2e_{23}, 2e_{13}, 2e_{12})$ where $e_{ij} = \frac{1}{2}(\partial_i u_j + \partial_j u_i)$, and $\partial_i \equiv \partial/\partial x_i$.

Orthotropic (or isotropic) homogeneous materials are considered, hence the stress tensor $\boldsymbol{\sigma}$ is given by Hooke's law

$$\boldsymbol{\sigma} = [C]\,\mathbf{e} \tag{1}$$

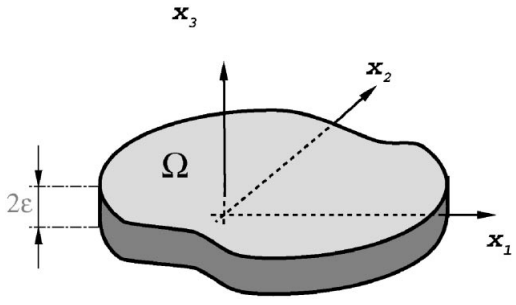

Figure 1. Typical plate of interest and notations.

where $[C]$ is a 6×6 (positive) symmetric matrix associated with the 3-D material constituting the domain, in the form

$$[C]=\begin{pmatrix} C_{11} & C_{12} & C_{13} & 0 & 0 & 0\\ & C_{22} & C_{23} & 0 & 0 & 0\\ & & C_{33} & 0 & 0 & 0\\ & & & C_{44} & 0 & 0\\ & & & & C_{55} & 0\\ & & & & & C_{66}\end{pmatrix} \tag{2}$$

In case the material is isotropic then

$$C_{11}=C_{22}=C_{33}=\frac{E(1-v)}{(1+v)(1-2v)},\qquad C_{12}=C_{13}=C_{23}=\frac{Ev}{(1+v)(1-2v)}$$

and

$$C_{44}=C_{55}=C_{66}=\frac{E}{2(1+v)}$$

Here E is the Young modulus and v is the Poisson ratio.

Denoting the material density by ρ, the sought vibration eigen-frequencies λ of the three-dimensional plate are the solutions of the following weak eigen-problem:

$$\begin{gathered}\text{Seek } \lambda>0 \text{ and } \mathbf{0}\neq\mathbf{u}\in\mathbf{V}(\Omega),\ \text{such that } \forall\mathbf{v}\in\mathbf{V}(\Omega)\\ \int\!\!\int_\omega\int_{-\varepsilon}^{\varepsilon}\mathbf{e}(\mathbf{u})^{\mathrm{T}}[C]\mathbf{e}(\mathbf{v})\,\mathrm{d}x_1\,\mathrm{d}x_2\,\mathrm{d}x_3=\lambda^2\int\!\!\int_\omega\int_{-\varepsilon}^{\varepsilon}\rho\,\mathbf{u}^{\mathrm{T}}\cdot\mathbf{v}\,\mathrm{d}x_1\,\mathrm{d}x_2\,\mathrm{d}x_3\end{gathered} \tag{3}$$

where

$$\mathbf{V}(\Omega)=\{\mathbf{v}\in[H^1(\Omega)]^3,\ \mathbf{v}=0 \text{ on } \partial\omega\times(-\varepsilon,\varepsilon)\}$$

$H^1(\Omega)$ being the usual Sobolev space.

The eigen-frequencies form an increasing sequence $n\mapsto\lambda_n^\varepsilon$ of positive numbers where we agree to repeat each eigen-frequency according to its multiplicity. There is no finite accumulation point. The superscript ε indicates that we fix the mid-surface ω and that we consider the eigen-frequencies as functions of the thickness ε.

Let S be the transverse symmetry operator defined for $\mathbf{u}=(u_1,u_2,u_3)$ by

$$\mathbf{u}\overset{S}{\longmapsto}((x_1,x_2,x_3)\mapsto(u_1(x_1,x_2,-x_3),u_2(x_1,x_2,-x_3),-u_3(x_1,x_2,-x_3))) \tag{4}$$

We note that

$$\int\!\!\int_\omega\int_{-\varepsilon}^{\varepsilon}\rho\mathbf{u}^{\mathrm{T}}\cdot\mathbf{v}\,\mathrm{d}x_1\,\mathrm{d}x_2\,\mathrm{d}x_3=\int\!\!\int_\omega\int_{-\varepsilon}^{\varepsilon}\rho(S\mathbf{u})^{\mathrm{T}}\cdot S\mathbf{v}\,\mathrm{d}x_1\,\mathrm{d}x_2\,\mathrm{d}x_3$$

and that for orthotropic materials

$$\int\int_\omega\int_{-\varepsilon}^{\varepsilon}\mathbf{e}(\mathbf{u})^{\mathrm{T}}[C]\,\mathbf{e}(\mathbf{v})\,\mathrm{d}x_1\,\mathrm{d}x_2\,\mathrm{d}x_3=\int\int_\omega\int_{-\varepsilon}^{\varepsilon}\mathbf{e}(S\mathbf{u})^{\mathrm{T}}[C]\mathbf{e}(S\mathbf{v})\,\mathrm{d}x_1\,\mathrm{d}x_2\,\mathrm{d}x_3$$

We deduce that each eigen-space determined by (3) can be split as the direct sum of a *bending* subspace (i.e. where the elements $\mathbf{u}$ satisfy $S\mathbf{u}=-\mathbf{u}$, in other words $\mathbf{u}$ are anti-symmetric in

respect to the mid-plane ω) and a *membrane* or *stretching* subspace (where $\mathbf{u}$ satisfy $S\mathbf{u} = \mathbf{u}$). Therefore for each fixed ε, each eigen-frequency in the sequence (λ_n^ε) is either bending or membrane.

2.2. Isotropic 3-D plate

For ease of presentation we fix the material density $\rho \equiv 1$. For isotropic materials it has been shown in References [1,2] that for each fixed rank n, for ε small enough λ_n^ε is a bending eigen-frequency and that $\lambda_n^\varepsilon/\varepsilon$ tends to the nth eigen-frequency, denoted by λ_n^{KL}, of the *Kirchhoff–Love dimensionally reduced model*

$$L^{\mathrm{KL}} := \frac{E\Delta^2}{3(1-\nu^2)} : H_0^2(\omega) \longrightarrow H^{-2}(\omega) \tag{5}$$

In Reference [2] it is proved that λ_n^ε has a power series expansion in terms of ε, i.e. there exist real coefficients $\lambda_{n,i}$ for $i \geqslant 1$ such that for any k

$$\lambda_n^\varepsilon = \varepsilon\lambda_{n,1} + \varepsilon^2\lambda_{n,2} + \cdots + \varepsilon^k\lambda_{n,k} + \mathcal{O}(\varepsilon^{k+1}) \tag{6}$$

Here, of course, $\lambda_{n,1}$ coincides with λ_n^{KL}. Following the analyses of Reference [2] (and see also Reference [3, Section 8]) we find the first two terms of the expansion of the *scaled eigen-values* Λ_n^ε

$$\Lambda_n^\varepsilon := (\lambda_n^\varepsilon/\varepsilon)^2 = \Lambda_{n,0} + \varepsilon\Lambda_{n,1} + \cdots + \varepsilon^k\Lambda_{n,k} + \mathcal{O}(\varepsilon^{k+1}) \tag{7}$$

The first term $\Lambda_{n,0}$ is the nth eigen-value of the Kirchhoff–Love model, i.e. $(\lambda_n^{\mathrm{KL}})^2$. As for the second term $\Lambda_{n,1}$, it is equal to

$$\Lambda_{n,1} = \frac{E}{3}\int_{\partial\omega} c^{\mathrm{b}}(\nu)|(\partial_1^2 + \partial_2^2)\zeta_{n,0}|^2 \,\mathrm{d}s \tag{8}$$

where $\zeta_{n,0} \in H_0^2(\omega)$ is the n^{th} eigen-function[†] of the Kirchhoff–Love model L^{KL} normalized in $L^2(\omega)$, and c^{b} is a coupling constant related to the structure of the first boundary layer term in the expansion of 3-D eigen-vectors. This coupling constant is positive and depends only on ν. See details in Appendix A.

We immediately deduce that $\lambda_{n,2} = \Lambda_{n,1}/(2\sqrt{\Lambda_{n,0}})$, and obtain

$$\lambda_{n,2} = \frac{E}{6\lambda_{n,1}}\int_{\partial\omega} c^{\mathrm{b}}(\nu)|(\partial_1^2 + \partial_2^2)\zeta_{n,0}|^2 \,\mathrm{d}s \tag{9}$$

2.3. Orthotropic 3-D plate

Stricto sensu, the eigenvalue expansion (7) is not known for non-isotropic plates. Nevertheless, *for clamped lateral boundary conditions*, it is possible to use all constructions in Reference [2] and to extend the results of isotropic plates to orthotropic plates. Details are provided in Appendix A.

[†]When λ_n^{KL} is a multiple eigen-frequency of L^{KL}, according to the constructions of Reference [2], extra criteria have to be applied for the determination of $\zeta_{n,0}$: the pair $(\zeta_{n,0}, \Lambda_{n,1})$ has to be an eigen-pair of a finite positive symmetric eigen-problem, see Appendix A.

We still fix the density to $\rho \equiv 1$. Then for fixed n, the n^{th} eigen-frequency has a power series expansion with respect to ε in the form (6) where $\lambda_{n,1} = \lambda_n^{\text{KL}}$ with the n^{th} eigen-frequency λ_n^{KL} of the *Kirchhoff–Love dimensionally reduced model* L^{KL} associated with material matrix $[C]$ on ω, cf. Reference [6]:

$$\begin{aligned} L^{\text{KL}} : H_0^2(\omega) &\longrightarrow H^{-2}(\omega) \\ \zeta &\longmapsto \tfrac{1}{3}(\widetilde{C}_{11}\partial_1^4 + \widetilde{C}_{22}\partial_2^4 + 2(\widetilde{C}_{12} + 2\widetilde{C}_{66})\partial_1^2\partial_2^2)\zeta \end{aligned} \tag{10}$$

where for $i, j \in \{1, 2, 6\}$, $\widetilde{C}_{ij}$ is defined as

$$\widetilde{C}_{ij} = C_{ij} - \frac{C_{i3}C_{j3}}{C_{33}} \tag{11}$$

Thus, according to (6), $\lambda_n^\varepsilon/\varepsilon \to \lambda_{n,1}$, as $\varepsilon \to 0$, i.e. the n^{th} eigen-frequency over ε must approach a constant value as the plate thickness tends to zero. This will be visualized by numerical examples.

As for the second term $\lambda_{n,2}$ in (6), it has an expression like (9) but with a *positive coupling function* defined on $\partial\omega$ and depending on the material matrix $[C]$:

$$\lambda_{n,2} = \frac{1}{2\lambda_{n,1}} \int_{\partial\omega} c^{\text{b}}([C]; s)|(\partial_1^2 + \partial_2^2)\zeta_{n,0}|^2 \, \mathrm{d}s \tag{12}$$

Therefore we expect, as noted in Reference [3], that $\varepsilon \mapsto \lambda_n^\varepsilon/\varepsilon$ is increasing for ε small enough. This will be visualized by numerical examples.

2.4. Eigen-frequencies of the Reissner–Mindlin plate model

For completeness of presentation, we provide herein the derivation of the weak eigen-problem for the R–M plate model made of orthotropic materials.

The displacement field under the R–M assumptions can be represented as

$$\begin{Bmatrix} u_1 \\ u_2 \\ u_3 \end{Bmatrix} = \begin{Bmatrix} -x_3\beta_1(x_\alpha) \\ -x_3\beta_2(x_\alpha) \\ w(x_\alpha) \end{Bmatrix} \tag{13}$$

where the index α denotes the values $\{1, 2\}$ corresponding to the in-plane variables. The in-plane functions $\beta_1(x_\alpha)$ and $\beta_2(x_\alpha)$ have the physical interpretation of rotations, while the function $w(x_\alpha)$ denotes the deflection of the mean surface of the plate. R–M displacement field assumption implies that *normals to the mean surface ω remain straight lines after deformation, but not necessary normals*. Thus, the strain vector $\mathbf{e}$ is

$$\begin{Bmatrix} e_1 \\ e_2 \\ e_3 \\ e_4 \\ e_5 \\ e_6 \end{Bmatrix} = \begin{Bmatrix} -x_3\partial_1\beta_1 \\ -x_3\partial_2\beta_2 \\ 0 \\ (\partial_2 w - \beta_2) \\ (\partial_1 w - \beta_1) \\ -x_3(\partial_2\beta_1 + \partial_1\beta_2) \end{Bmatrix} \tag{14}$$

and as noted $e_3 = 0$.

The second important assumption for constructing the R–M plate model, is that σ_3 *is negligible*. Therefore one introduces the constraint $\sigma_3 = 0$ in the model. Writing (1) in index notation, we obtain

$$\sigma_i = C_{ij} e_j, \quad i,j = 1,\ldots,6 \tag{15}$$

Due to the constraint $\sigma_3 = 0$, i.e. $C_{3j} e_j = 0$, we substitute e_3 by $-\sum_{k\neq 3} C_{3k} e_k / C_{33}$ in (15) except for $i = 3$, and we obtain

$$\sigma_i = \sum_{j\neq 3} \left(C_{ij} - \frac{C_{i3} C_{3j}}{C_{33}} \right) e_j, \quad i,j = 1,2,4,5,6 \tag{16}$$

We note that for $i,j = 1,2,6$, the new material coefficients $C_{ij} - C_{i3}C_{3j}/C_{33}$ are nothing else than $\widetilde{C}_{ij}$ already introduced in notation (11). Based on (16) we obtain a modified Hooke's law, connecting the stress vector $(\sigma_1, \sigma_2, \sigma_4, \sigma_5, \sigma_6)$ with the strain vector $(e_1, e_2, e_4, e_5, e_6)$. The 5×5 material matrix $[\widetilde{C}] = (\widetilde{C}_{ij})_{i,j=1,2,4,5,6}$ obtained is

$$[\widetilde{C}] = \begin{pmatrix} C_{11} - \dfrac{C_{13}^2}{C_{33}} & C_{12} - \dfrac{C_{13}C_{23}}{C_{33}} & 0 & 0 & 0 \\ & C_{22} - \dfrac{C_{23}^2}{C_{33}} & 0 & 0 & 0 \\ & & C_{44} & 0 & 0 \\ & & & C_{55} & 0 \\ & & & & C_{66} \end{pmatrix} \tag{17}$$

To account for a correction in the shear stresses σ_{13} and σ_{23} to better represent the fully 3-D stresses, the material matrix entries $\widetilde{C}_{44}$ and $\widetilde{C}_{55}$ are changed by introducing the so-called shear correction factor κ:

$$\widetilde{C}_{44} = \kappa C_{44}, \qquad \widetilde{C}_{55} = \kappa C_{55}$$

By properly choosing κ, either the energy of the R–M solution, or the deflection w can be optimized with respect to the fully 3-D plate. The smaller the ε, the smaller the influence of κ on the results. For the isotropic case two possible κ's are (see details in Reference [7]):

$$\kappa_{\text{Energy}} = \frac{5}{6(1-\nu)}$$
$$\kappa_{\text{Deflection}} = \frac{20}{3(8-3\nu)}$$

For modal analysis, it is not clear that an optimal value of κ is available. A value of $\kappa = 5/6$ is frequently used in engineering practice. It is important to note that for orthotropic materials the value of κ is set to 1.

Defining the vector $\boldsymbol{\beta} = (\beta_1(x_\alpha), \beta_2(x_\alpha))^{\mathrm{T}}$ and the vector $\boldsymbol{\eta} = (\eta_1(x_\alpha), \eta_2(x_\alpha))^{\mathrm{T}}$, and assuming $\rho \equiv 1$ as in the previous subsections, we can introduce the following two bi-linear forms for

the R–M plate model:

$$\mathscr{A}(\boldsymbol{\beta},w,\boldsymbol{\eta},v)=\frac{\varepsilon^3}{3}\int\!\!\int_\omega \widetilde{C}_{11}\partial_1\beta_1\,\partial_1\eta_1+\widetilde{C}_{12}(\partial_1\beta_1\,\partial_2\eta_2+\partial_2\beta_2\,\partial_1\eta_1)$$
$$+\widetilde{C}_{22}\partial_2\beta_2\,\partial_2\eta_2+\widetilde{C}_{66}(\partial_2\beta_1+\partial_1\beta_2)(\partial_2\eta_1+\partial_1\eta_2)\,\mathrm{d}x_1\,\mathrm{d}x_2$$
$$+\varepsilon\int\!\!\int_\omega \widetilde{C}_{44}(\partial_2 w-\beta_2)(\partial_2 v-\eta_2)+\widetilde{C}_{55}(\partial_1 w-\beta_1)(\partial_1 v-\eta_1)\,\mathrm{d}x_1\,\mathrm{d}x_2 \quad (18)$$

$$\mathscr{M}(\boldsymbol{\beta},w,\boldsymbol{\eta},v)=\frac{\varepsilon^3}{3}\int\!\!\int_\omega(\beta_1\eta_1+\beta_2\eta_2)\,\mathrm{d}x_1\,\mathrm{d}x_2+\varepsilon\int\!\!\int_\omega wv\,\mathrm{d}x_1\,\mathrm{d}x_2 \quad (19)$$

Using the above definitions, the weak eigen-problem for the *clamped* R–M plate model is

$$\text{Seek } \widetilde{\lambda}>0 \text{ and } \mathbf{0}\neq(\boldsymbol{\beta},w)\in\mathbf{V}^{\mathrm{RM}}(\omega)$$

such that

$$\mathscr{A}(\boldsymbol{\beta},w,\boldsymbol{\eta},v)=\widetilde{\lambda}^2\mathscr{M}(\boldsymbol{\beta},w,\boldsymbol{\eta},v),\quad \forall(\boldsymbol{\eta},v)\in\mathbf{V}^{\mathrm{RM}}(\omega) \quad (20)$$

where

$$\mathbf{V}^{\mathrm{RM}}(\omega)=\{(\boldsymbol{\beta},w)\in[H^1(\omega)]^3,\ \beta_1=\beta_2=w=0 \text{ on } \partial\omega\}$$

The solution of (20) provides the Reissner–Mindlin eigen-frequencies, which form for each ε an increasing sequence denoted by $(\widetilde{\lambda}_n^\varepsilon)_n$, where we perform the same convention of repeating according to the multiplicity as before.

By similar (and much easier) constructions than in Reference [2], we can prove that the nth R–M eigen-frequency has a power series expansion in ε

$$\widetilde{\lambda}_n^\varepsilon=\varepsilon\widetilde{\lambda}_{n,1}+\varepsilon^2\widetilde{\lambda}_{n,2}+\cdots+\varepsilon^k\widetilde{\lambda}_{n,k}+\mathcal{O}(\varepsilon^{k+1}) \quad (21)$$

Here, the first coefficient $\widetilde{\lambda}_{n,1}$ is equal to its counterpart $\lambda_{n,1}$ in (6), i.e. the n^{th} K–L eigen-frequency.

In the 3-D eigen-frequency asymptotics (6), the presence of a non-zero second coefficient $\lambda_{n,2}$ is a consequence of the presence of the in-plane boundary layer components Φ_α^1 at the second rank in (A2). But, for the *clamped R–M model*, it is known, see References [4, 5], that the boundary layer series starts one rank further. That is why we can prove, see Appendix B, that

$$\widetilde{\lambda}_{n,2}=0 \quad (22)$$

Therefore, from the asymptotic expansion point of view, the approximation of the 3-D eigen-frequencies by R–M eigen-frequencies is only correct at the order 1.

3. FRAMEWORK OF NUMERICAL INVESTIGATION

Of major interest is the question whether the R–M eigen-frequencies are a good approximation of the 3-D eigen-frequencies. To address this question we define the *relative error* for the n^{th} eigen-frequency as follows:

$$\delta_n^\varepsilon \stackrel{\text{def}}{=} \frac{\lambda_n^\varepsilon - \widetilde{\lambda}_n^\varepsilon}{\lambda_n^\varepsilon} \tag{23}$$

Relying on the previous qualitative mathematical theory, it is now natural for us to address the following questions:

(a) How close are the R–M eigen-frequencies to their 3-D counterparts? Which shear correction factor should be used so as to obtain the 'best' eigen-frequencies for the R–M plate models? How small should the ratio between ε and the other plate dimensions be so that the R–M eigen-frequencies approximate the 3-D ones well?

(b) From asymptotics (12) and (22), we see that

$$\delta_n^\varepsilon \simeq \frac{\varepsilon\lambda_{n,2}}{\lambda_{n,1}}$$

Thus the question is how big is $\varepsilon\lambda_{n,2}$ compared with $\lambda_{n,1}$ for small, but non-zero ε? Especially, are there material properties so that $\lambda_{n,1}$ is of the same order of magnitude as $\varepsilon\lambda_{n,2}$ for a given small ε?

(c) In this connection, what is the influence of the geometrical shape of the plate boundary and the material properties on $\lambda_{n,2}$?

To address the above questions, which are of a quantitative nature, three-dimensional plates are considered and analysed from the numerical approximation point of view by the *p*-version of the finite element method.

3.1. Three-dimensional plates

We consider a rectangular plate, with or without a circular hole, having dimensions of $2 \times 1 \times 2\varepsilon$, as shown in Figure 2. The lateral boundaries of the plate are clamped, $\mathbf{u} = \mathbf{0}$ along *AEFG*, and in the case of the plate with the hole as well, the boundaries along the circular hole are clamped. Since only bending eigen-frequencies are sought, we have to consider anti-symmetric modes with respect to x_3. This is accomplished by taking only the upper half of the plate $\varepsilon > x_3 > 0$ as the computational domain, with anti-symmetric boundary condition $u_1 = u_2 = 0$ on the entire mid-surface $x_3 = 0$. The first bending eigen-frequency of the whole plate is symmetric with respect to $x_1 = 1$ and $x_2 = 1/2$ therefore, it is exactly the one obtained as the first eigen-frequency of the one-eighth computational domain. Thus, we further reduce the computational cost and compute the first three eigen-frequencies which are symmetric along $x_1 = 1$ and $x_2 = 1/2$. The computational domain is therefore one-eighth of the original plate, the shaded domain *ABCD* (resp. *ABCC′D* for the plate with a circular hole), with clamped boundary conditions along the lateral boundaries *AB* and *AD* (and *CC′* respectively), symmetric boundary conditions along the other two lateral boundaries, i.e. $u_1 = 0$ along *BC* and $u_2 = 0$ along *CD* (resp. *C′D*), and anti-symmetric boundary conditions on the plane $x_3 = 0$.

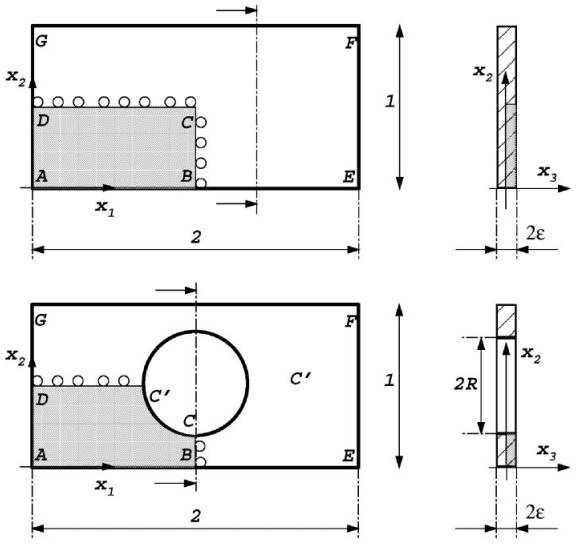

Figure 2. Rectangular plate under consideration.

Four different material properties are investigated, two of which are isotropic and the other two orthotropic. For all the cases the density is taken as $\rho = 1$.

Name	Young Modulus E	Poisson ratio ν
Isotropic	0.854	0.382
Almost incompressible	1	0.49

Name	$C_{11} = C_{22}$	C_{12}	$C_{13} = C_{23}$	C_{33}	$C_{44} = C_{55} = C_{66}$
Strongly orthotropic	11	9.9	1	0.1	1
Orthotropic	3	1.5	1	0.5	1

A three-dimensional p-version finite element model is constructed having two elements in the thickness direction, x_3, and three elements in the x_1 and x_2 directions. In the neighbourhood of the edges, the mesh is graded so that there is an element of dimension ε each. The finite element model is constructed parametrically so that the value of ε may vary, and we change it from 0.1 to 0.001. For the plate with a circular hole, three radii are analysed: $R = 0.2,\ 0.3$ and 0.4. In Figure 3 the mesh used for the various problems of interest is presented for plates of half-thickness $\varepsilon = 0.1$.

The p-level over each element has been increased from 1 to 8 and the trunk space has been used (see Reference [8]). For the rectangular plate (with 18 hexahedral elements) there are 4068 degrees of freedom at $p = 8$, and the eigen-frequencies are converged to within a relative error of less than 0.5 per cent at $p = 8$ for most ε. An advantage of using p-version finite element methods is the possibility of having 'needle elements' in the boundary layer zone with aspect ratios as large as 1000 without significant degradation in the numerical performance. An *exponential convergence rate* is obtained (due to the use of high-order elements) and the

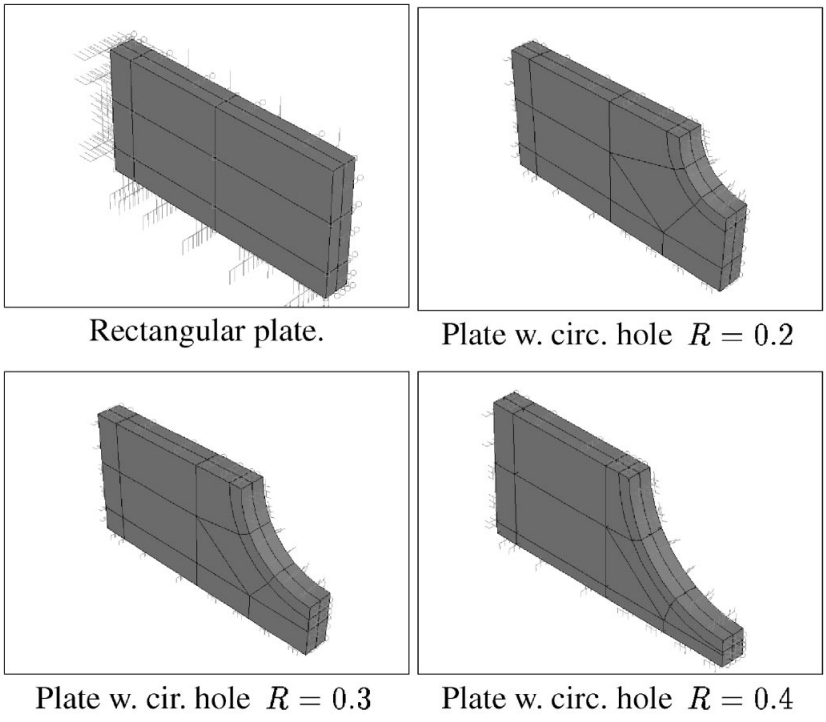

Figure 3. Finite element meshes for 3-D analysis with $\varepsilon = 0.1$.

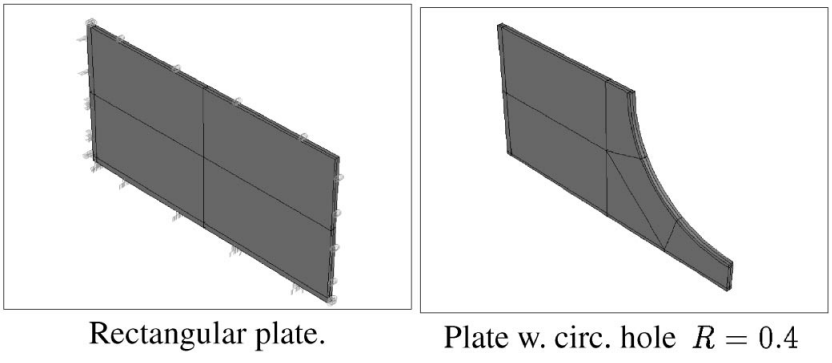

Figure 4. Finite element meshes for 3-D analysis with $\varepsilon = 0.01$.

convergence of the eigen-frequencies (the first three of them) has been examined in order to evaluate the reliability of the numerical results.

In Figure 4 we present the finite element mesh for the case where $\varepsilon = 0.01$. As may be noticed the boundary layer elements are changed according to the plate thickness. Although almost not visible, there are two elements across the thickness and one element each of dimension ε in the neighbourhood of the boundary.

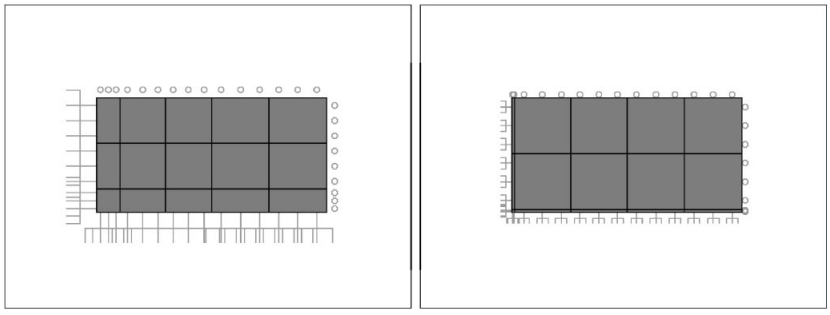

Figure 5. Finite element meshes for the rectangular R–M plate model.

All finite element computations are done within the finite element code Stress Check[‡].

3.2. *R–M plate models*

Finite element models of mid-surfaces of the 3-D plate have been constructed similar to the 3-D meshes, where one fourth of the plate has been considered for computing the symmetric eigen-frequencies. Again, a layer of one element along the plate boundary of width equal to ε is present. An example of the meshes for the R–M plate with $\varepsilon = 0.1$ and 0.01 is shown in Figure 5. One can specify three different shear correction factors used in conjunction with the R–M plate model made of an isotropic material: κ_{Energy}, $\kappa_{\text{Deflection}}$ or $\kappa = 1$. For orthotropic material only $\kappa = 1$ is available in the code that we use. Again, we increase the polynomial degree over each element from 1 to 8 and observe an exponential convergence in the eigen-frequencies (usually less than 0.1 per cent relative error for most ε values at $p = 8$ with 2816 degrees of freedom).

4. QUANTITATIVE COMPARISON BETWEEN 3-D AND R–M EIGEN-FREQUENCIES

We give the results of numerical experimentations in the rectangular plate for the four different material laws introduced in the previous section. Then we provide a few results on the influence of the shape of the mid-surface.

4.1. *The standard isotropic material*

This subsection is devoted to the rectangular plate with the 'isotropic' material properties. We investigate which of the three κs, used for the R–M plate model, provide the closest eigen-frequencies compared with their 3-D counterparts. We plot the first three symmetric eigen-frequencies/ε vs the plate half thickness ε in Figure 6.

[‡] Stress Check is a trade mark of Engineering Software Research and Development, Inc., 10845 Olive Blvd., Suite 170, St. Louis, MO 63141, U.S.A.

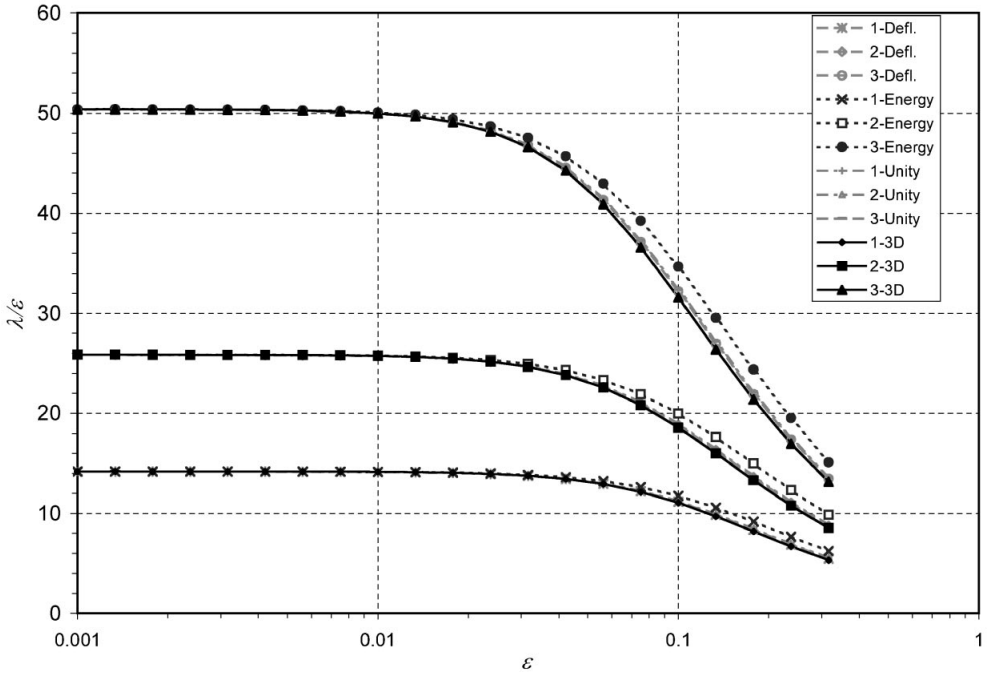

Figure 6. First three symmetric eigen-frequencies for 'isotropic' rectangular plate: 3-D vs R–M model with different κ's.

As expected by the mathematical analysis, indeed $\lambda_n/\varepsilon \to \lambda_{n,1}$ as $\varepsilon \to 0$, and also $\widetilde{\lambda}_n \to \lambda_n$ regardless of the κ used.

To better visualize the difference between $\widetilde{\lambda}_n$ and λ_n we provide in Figure 7 the relative error δ_1^ε for the first eigen-frequency for the three choices of κ. The representation of relative errors δ_2^ε and δ_3^ε for the second and third eigen-frequencies is very similar.

At the observation scale of Figure 7, it seems that $\kappa_{\text{Deflection}}$ is the 'best' κ from the three investigated, in the sense that $\widetilde{\lambda}_n$ is the closest to λ_n for all investigated ε. Again at this observation scale, no linear dependence is visible (we cannot 'see' $\lambda_{n,2}$).

Using $\kappa_{\text{Deflection}}$ for the 'isotropic' material, the relative error for the first three eigen-frequencies is negligible (less than 0.12%) for thin plates with a slender ratio of less than 1 per cent, and for moderately thick plates (thickness about 5% compared to other plate dimensions) is smaller than 0.2%.

Now, if we magnify the ordinates of Figure 7 by a factor 100, we obtain Figure 8, where the expected increase of the eigen-frequency with ε (due to the non-zero factor $\lambda_{1,2}$) is clearly visible. In this 'asymptotic' region, the shear correction factor κ_{Energy} is the best one.

4.2. Almost incompressible materials

The numerical values of the function $\nu \mapsto c^{\text{b}}(\nu)$, see Appendix A, suggest that the difference between λ_n and $\widetilde{\lambda}_n$ should be much more pronounced as ν approaches 0.5. Herein we

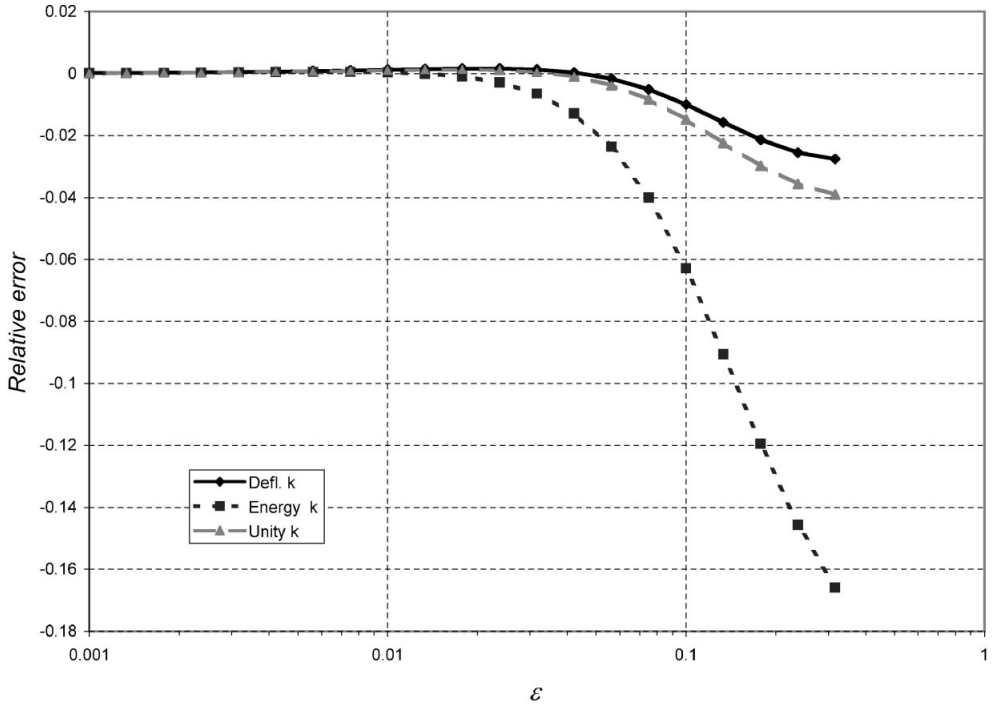

Figure 7. Relative error for the first eigen-frequency: 3-D vs R–M model with different κ's.

investigate the rectangular plate discussed in Section 4.1 only with 'almost incompressible' material properties. In Figure 9 we provide the relative error for the first eigen-frequency with the different shear correction factors. Comparing with Figure 7 one can note the more pronounced difference between the R–M and 3-D eigen-frequencies as expected. In this case, a relative error of almost 0.6% is obtained for the first eigen-frequency at $\varepsilon \approx 0.03$.

We magnify the ordinates of Figure 9, to obtain Figure 10. Here again we see, as in the case of isotropic material in Figure 8, that in the 'asymptotic' region, the shear correction factor κ_{Energy} is the best one.

4.3. Orthotropic materials

We herein investigate the influence of the material law (orthotropicity) on the eigen-frequencies, based on the rectangular plate model. The material properties are those defined as 'orthotropic', and in Figure 11 we present the first symmetric three eigen-frequencies over ε vs ε for the 3-D and R–M plate. The relative error is presented in Figure 12. The relative error for the first eigen-frequency is around 5% at $\varepsilon \approx 0.07$, and increases up to 8% around $\varepsilon \approx 0.18$. Although the behaviour of the eigen-frequencies compared to the 'isotropic' plates is the same, we obtain herein a relative error which is larger by an order of magnitude compared to the isotropic case.

Plotting the relative error vs ε (not logarithmic scale), for $\varepsilon < 0.03$, a linear curve for $\varepsilon \to 0$ is visible as seen in Figure 13, supporting the asymptotic behaviour (6).

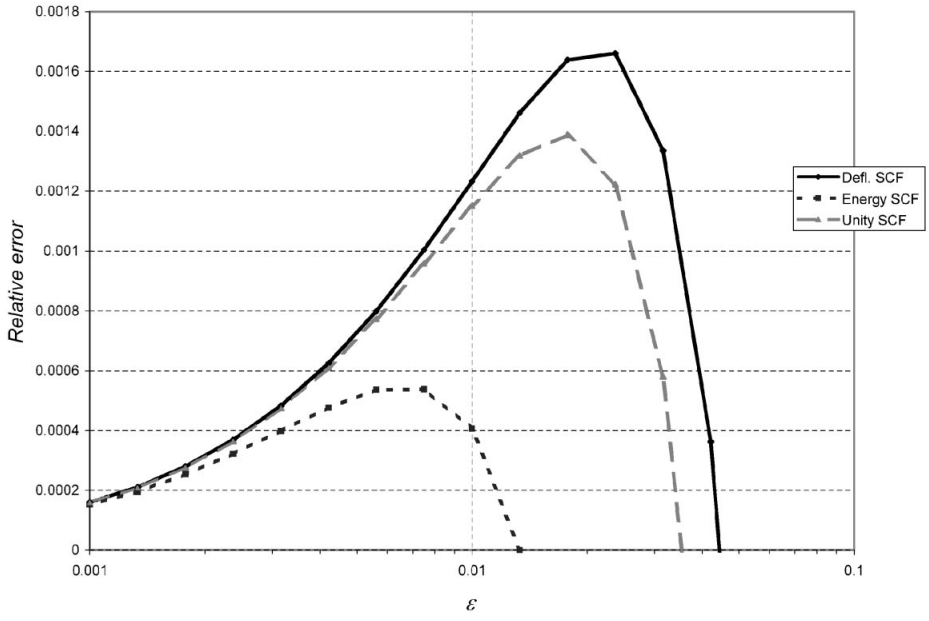

Figure 8. Zoom view of the relative error for the first eigen-frequency: 3-D vs R–M model with different κ's.

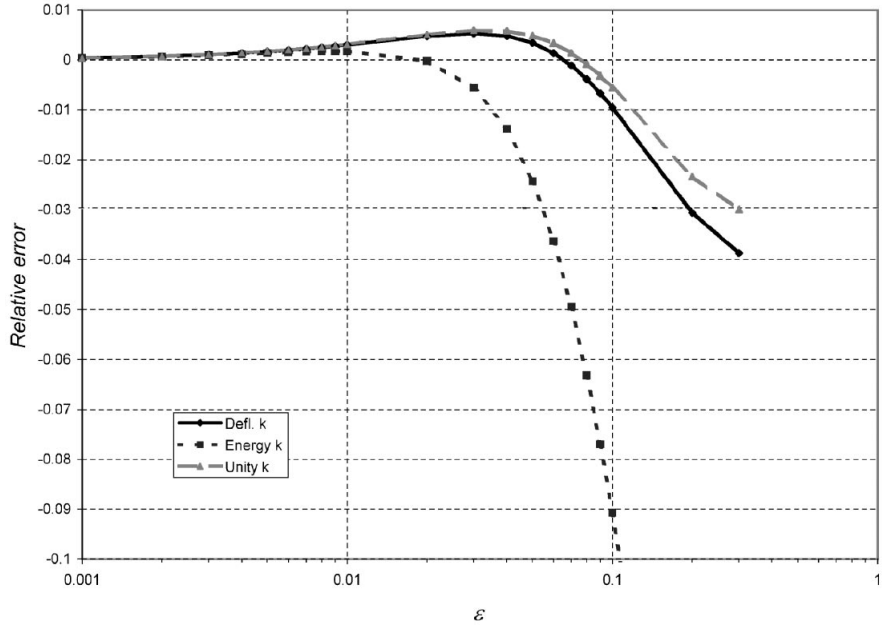

Figure 9. Relative error for the first eigen-frequency: 3-D vs R–M model with different κ's of 'almost incompressible material'.

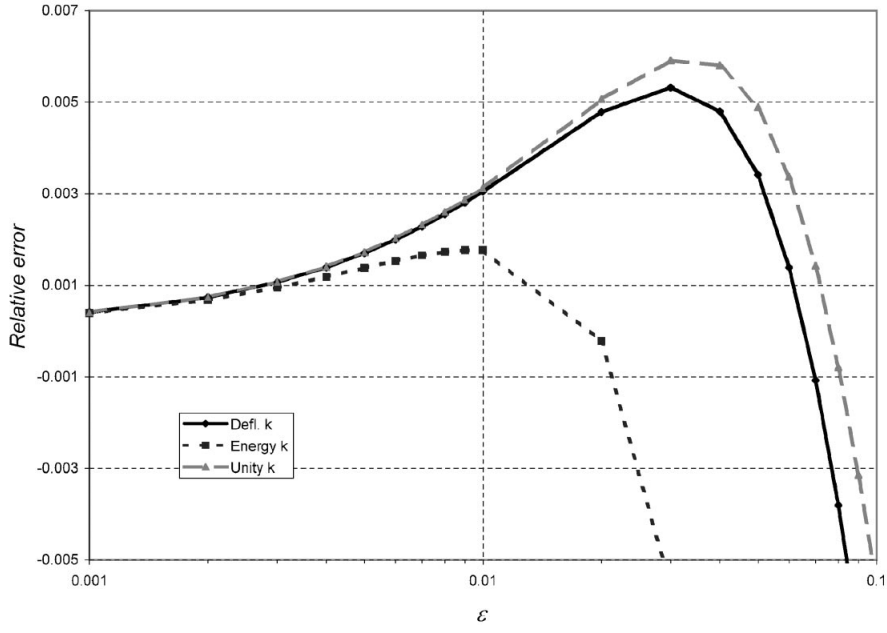

Figure 10. Zoom view of relative errors for the first eigen-frequency of 'almost incompressible material'.

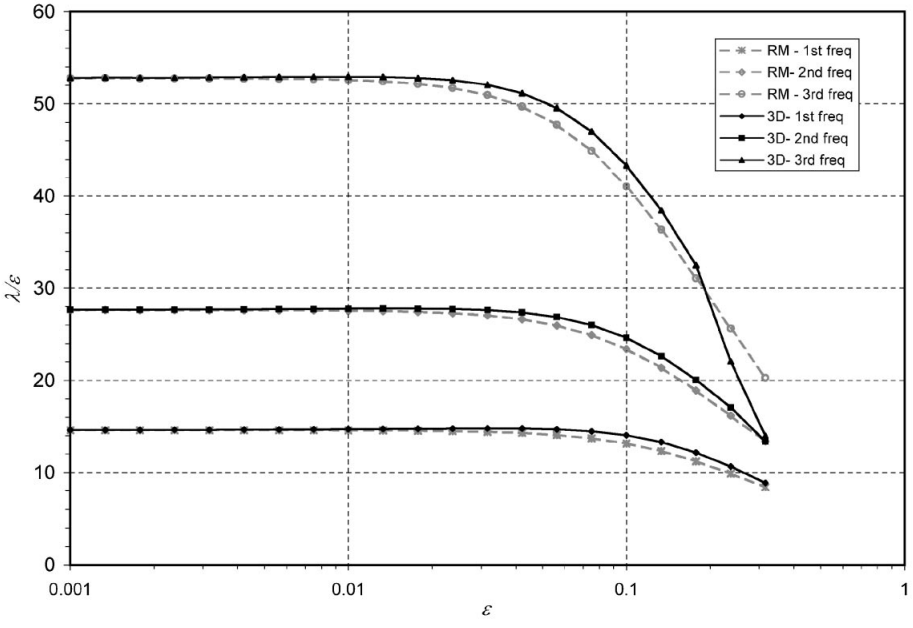

Figure 11. First three symmetric eigen-frequencies for 'orthotropic' rectangular plate: 3-D vs R–M model.

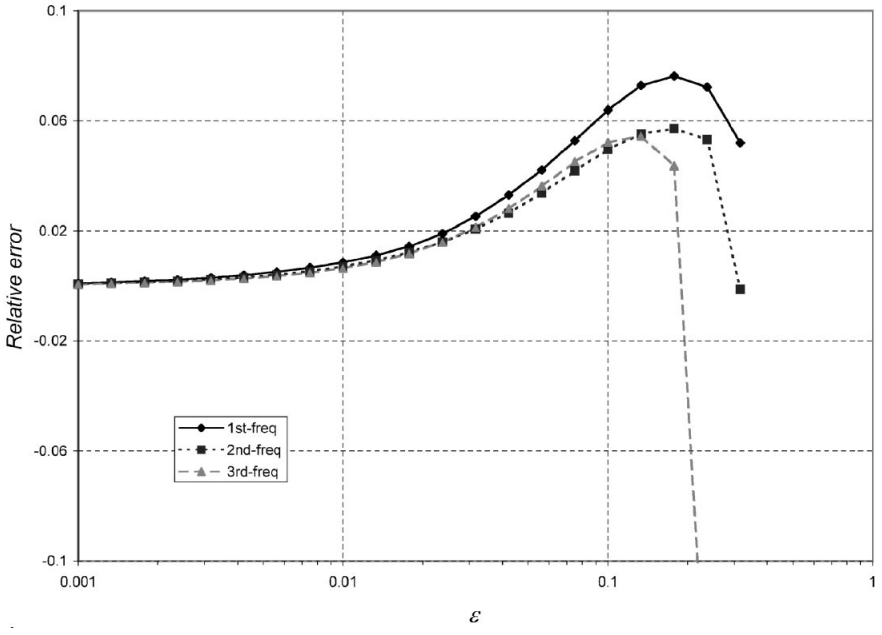

Figure 12. Relative error of the first three symmetric eigen-frequencies: 3-D vs R–M model made of 'orthotropic material'.

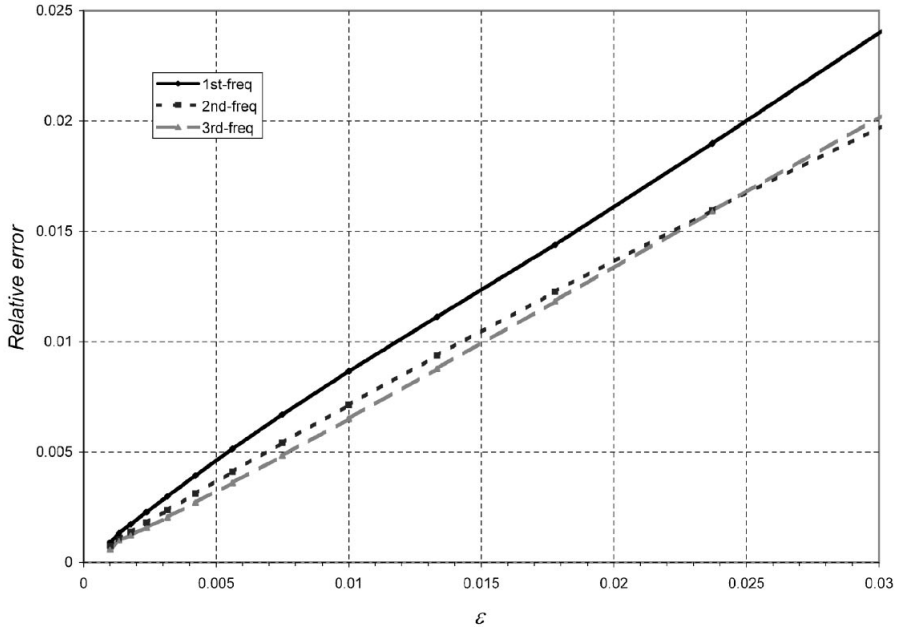

Figure 13. Relative error (linear graph) of the first three symmetric eigen-frequencies: 3-D vs R–M model made of 'orthotropic material'.

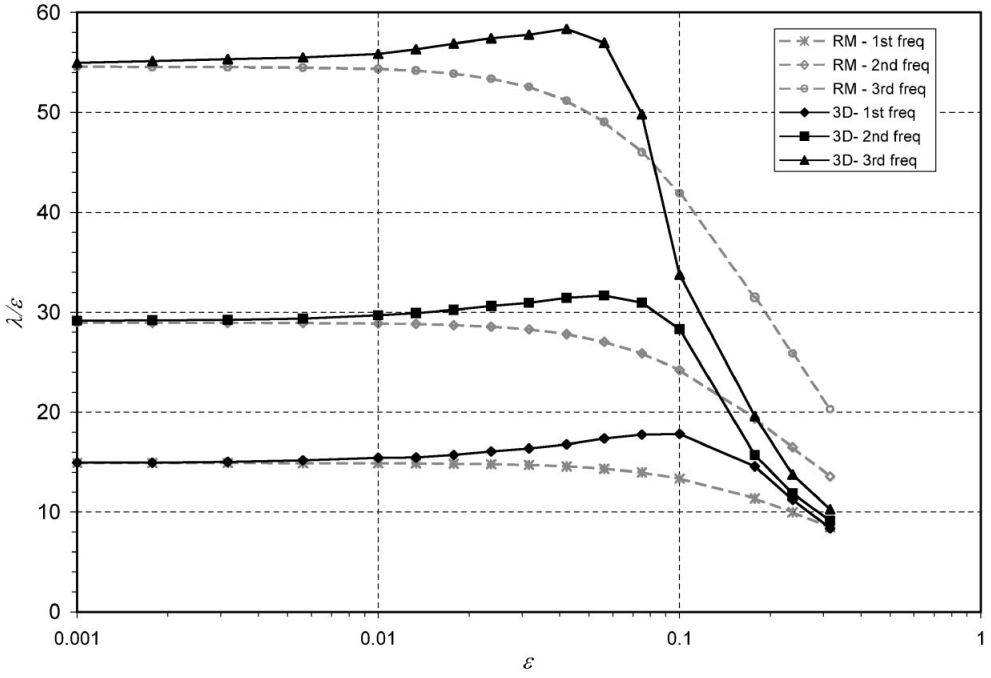

Figure 14. First three symmetric eigen-frequencies over ε for 'strongly orthotropic' rectangular plate: 3-D vs R–M model.

4.4. *Strongly orthotropic materials*

For the 'strongly orthotropic' plate, the boundary layer effect on the eigen-frequencies should be the most pronounced. In Figure 14 we present the first three symmetric eigen-frequencies over ε vs ε, as obtained from the 3-D analysis compared to those obtained by the R–M plate analysis with $\kappa = 1$. The 3-D eigen-frequencies over ε clearly tend to a limit as $\varepsilon \to 0$, and the values of λ_n/ε increase as ε increases up to $\varepsilon \approx 0.05$. The relative error is presented in Figure 15. A very large relative error of 25% is visible for the first eigen-frequency at $\varepsilon = 0.1$. This is a significant deviation whereas the R–M model underestimates the 'true' 3-D by 25%, and is attributed to the boundary layer effect.

4.5. *The effect of the shape of* $\partial\omega$

The mathematical analysis demonstrates that the 3-D eigen-frequencies are clearly sensitive to the shape of the mid-surface boundary. To quantify this effect we analyse the rectangular plate having a hole in its centre of increasing radii, as presented in Figure 3. Since the most pronounced effect between the 3-D and R–M plate eigen-frequencies is observed for the 'strongly orthotropic' material, we herein use the same material properties. The lowest (first) eigen-frequency over ε vs ε is plotted in Figure 16 for the rectangular plate without the whole, and for the plate with a hole of radius $R = 0.2, 0.3$, and 0.4.

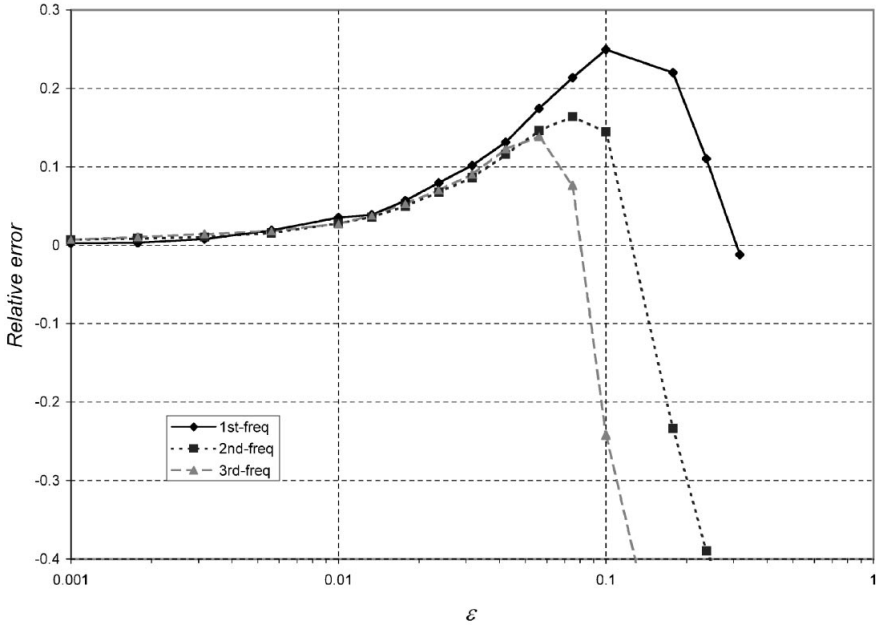

Figure 15. Relative error of the first three symmetric eigen-frequencies: 3-D vs R–M model made of 'strongly orthotropic material'.

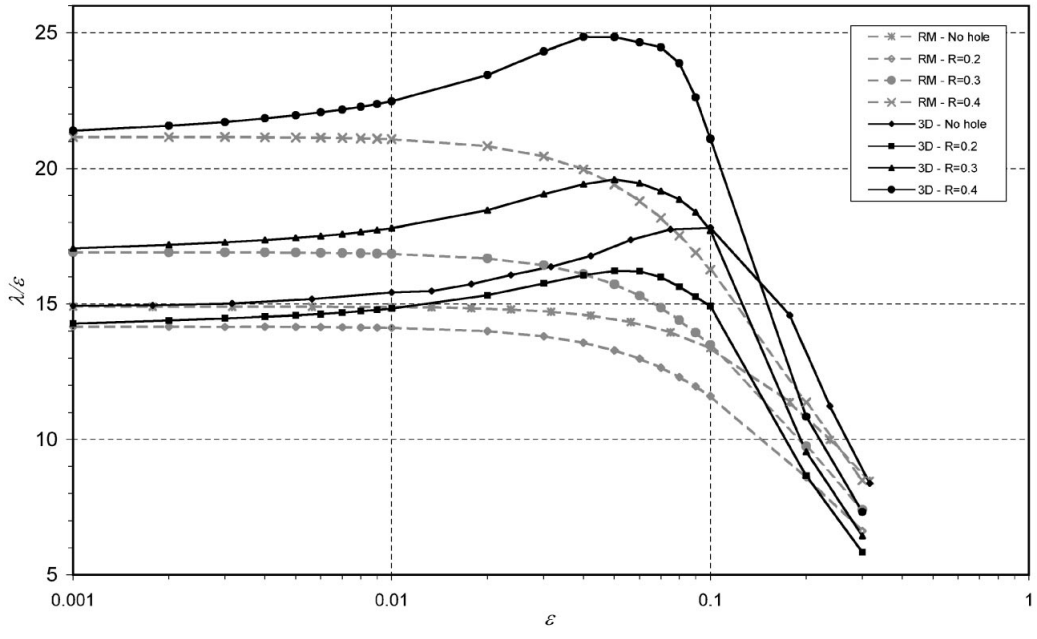

Figure 16. First eigen-frequency for a 'strongly orthotropic' plate with a hole of different radii: 3-D vs R–M model.

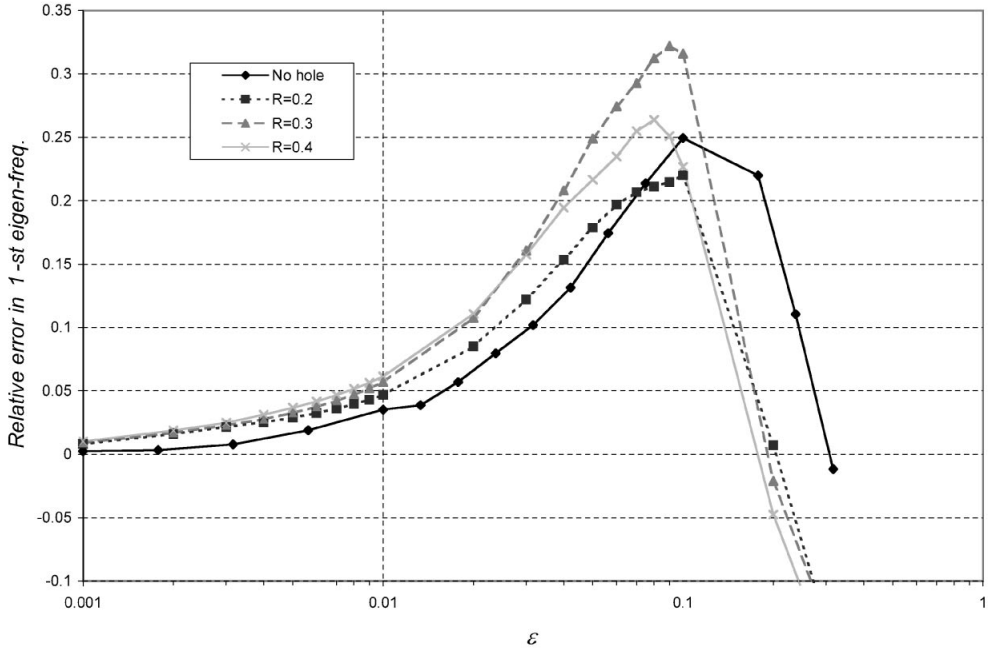

Figure 17. Relative error of the first eigen-frequency for a 'strongly orthotropic' plate with a hole of different radii.

The influence of the hole (the boundary layer effect is increased) is better seen when observing the relative error in the first eigen-frequency as a function of ε in Figure 17.

One can note that for the plate with a hole with $R = 0.3$ the relative error may be beyond 30% for $\varepsilon \approx 0.07$. On the other hand, there does not seem to be a clear connection between the length of the clamped boundary layer and the increase in the relative error. In fact, the relative error is larger for the plate without the hole in comparison with the plate having a hole of radius $R = 0.2$, however, the situation is reversed when comparing the rectangular plate with the one having a hole of radius $R = 0.3$.

5. SUMMARY AND CONCLUSIONS

The eigen-frequencies computed by using the Reissner–Mindlin plate model are frequently used in engineering practice as an approximation to the three-dimensional plate eigen-frequencies for relatively thin elastic plates. In this paper, we have explicitly provided the asymptotic behaviour of the eigen-frequencies as the thickness of the plate goes to zero, both for the R–M and 3-D plates made of either isotropic or orthotropic materials. The results for R–M and 3-D orthotropic plates are new. The 3-D and R–M asymptotics have a common first term but differ in their second terms.

The qualitative mathematical description is supported by quantitative numerical data obtained by the p-version finite element method for clamped plates. It was shown that for

isotropic materials and relatively thin plates the Reissner–Mindlin eigen-frequencies provide a good approximation to the three-dimensional eigen-frequencies. It was also demonstrated that for isotropic materials, no shear correction factor is known to be optimal in the sense that it provides the best approximation of the R–M eigen-frequencies to their 3-D counterparts uniformly (for all thicknesses range).

For some orthotropic materials we have shown relative errors between the R–M eigen-frequencies and their 3-D counterparts of an order of 30% even for relatively thin plates. This imposes a serious question mark on the relevance of the R–M eigen-analysis for plates made of orthotropic material. We also studied the influence of the shape of the mid-surface boundary on the errors in R–M eigen-frequencies.

APPENDIX A: 3-D EIGEN-VALUES—ASYMPTOTICS FOR ORTHOTROPIC PLATES

Herein, the results and constructions of Reference [2], which are valid for isotropic materials, are adapted to orthotropic materials. We explain in detail the formula for the second term in the asymptotics, which is left implicit in Reference [2].

A.1. Third-order ansatz

Let $X_3 := x_3/\varepsilon$ be the scaled transverse variable. Let (r,s) be boundary fitted co-ordinates along $\partial\omega$ in the mid-plane, with r the inward distance to $\partial\omega$ and s an arc-length co-ordinate along $\partial\omega$. Then $-\partial_r$ is the outward normal derivative along $\partial\omega$. Let furthermore $R := r/\varepsilon$ be the scaled distance to the boundary $\partial\omega$.

For ε small enough, there exists a 3-D eigenvector $\mathbf{u}^\varepsilon = (u_1^\varepsilon, u_2^\varepsilon, u_3^\varepsilon)$ associated with λ_n^ε with a two-scale asymptotic expansion (outer and inner expansion terms) starting with

$$u_3^\varepsilon = \zeta[\varepsilon] + \varepsilon^2\left(\frac{X_3^2}{2} - \frac{1}{6}\right)\frac{(C_{13}\partial_1^2 + C_{23}\partial_2^2)\zeta[\varepsilon]}{C_{33}} + \varepsilon^2(\Phi_3^1\zeta[\varepsilon])(s,R,X_3) + \mathcal{O}(\varepsilon^3) \tag{A1}$$

and for the in-plate components, $\alpha = 1,2$

$$u_\alpha^\varepsilon = -\varepsilon X_3\partial_\alpha\zeta[\varepsilon] + \varepsilon^2(\Phi_\alpha^1\zeta[\varepsilon])(s,R,X_3) + \mathcal{O}(\varepsilon^3) \tag{A2}$$

where the '*generator*' $\zeta[\varepsilon] = \zeta[\varepsilon](x_1,x_2) = \zeta_0 + \varepsilon\zeta_1 + \varepsilon^2\zeta_2 + \cdots$ is a (scalar) *formal series solution* of the dimensionally reduced eigenvalue equation (A3) below, and $\Phi^1 : \zeta \mapsto (\Phi^1\zeta)(s,R,X_3)$ is a three-component boundary layer operator.

The PDE operator $P(\partial_1,\partial_2)$ in the second term of (A1) can be found in the asymptotics for *monoclinic* materials in Reference [6, Section 2.3]. Note that for isotropic materials, this operator reduces to

$$\frac{C_{13}\partial_1^2 + C_{23}\partial_2^2}{C_{33}} = \frac{\nu}{1-\nu}(\partial_1^2 + \partial_2^2)$$

The equation to be satisfied by $\zeta[\varepsilon]$ in ω has the form

$$L[\varepsilon]\zeta[\varepsilon] = \Lambda[\varepsilon]\zeta[\varepsilon] \quad \text{in } \omega \tag{A3}$$

Here $L[\varepsilon]$ is an operator formal series $\sum_{j\geqslant 0}\varepsilon^j L_j$. The term of order 0 is $L_0 = L^{\mathrm{KL}}$ defined in (5), cf. [6, Section 2.3] and $L_1 = 0$. The solution of eigen-problem (A3) provides the series $\Lambda[\varepsilon]$ (terms of the asymptotics of Λ_n^ε) as defined in (7). Equation (A3) is completed by boundary conditions on $\partial\omega$ which can also be written as a formal series equation in the form $\gamma[\varepsilon]\zeta[\varepsilon] = 0$.

A.2. The first two eigen-problems for the generator

As we are interested in Λ_0 and Λ_1, it is enough to consider the first two terms in $\zeta[\varepsilon]$, say $\zeta_0 + \varepsilon\zeta_1$. The boundary conditions on $\zeta_0 + \varepsilon\zeta_1$ are obtained by considering ansatz (A1)–(A2), and looking for zero Dirichlet traces up to the order ε^2.

Considering the first terms in (A1) and (A2), we see that the boundary conditions on ζ_0 are $\zeta_0 = 0$ and $\partial_r\zeta_0 = 0$ on $\partial\omega$. With the first relation obtained from (A3) we have

$$L^{\mathrm{KL}}\zeta_0 = \Lambda_0\zeta_0 \quad \text{in} \quad \omega \qquad \text{and} \qquad \zeta_0,\ \partial_r\zeta_0 = 0 \quad \text{on } \partial\omega \tag{A4}$$

In order to obtain the boundary conditions for the next term in the asymptotics, ζ_1, one has to recall the procedure for obtaining the first boundary layer term $\Phi^1\zeta_0$.

Let $B(\partial_1, \partial_2, \partial_3)$ and $G(\partial_1, \partial_2, \partial_3)$ be the interior operator and the traction operators on the upper and lower faces of the plate, associated with the left-hand side of (3). Let moreover, $(n_1(s), n_2(s))$ be the components of the inward unit normal to $\partial\omega$. Then there holds

$$\partial_1 = n_1\partial_r + n_2\partial_s \quad \text{and} \quad \partial_2 = n_2\partial_r - n_1\partial_s \quad \text{on } \partial\omega$$

For each fixed $s \in \partial\omega$, the leading boundary layer operators are defined as

$$\mathscr{B}(s; \partial_R, \partial_{X_3}) := B(n_1(s)\partial_R, n_2(s)\partial_R, \partial_{X_3}) \quad \text{in the half-strip} \quad (0,\infty)\times(-1,1)$$

and

$$\mathscr{G}(s; \partial_R, \partial_{X_3}) := G(n_1(s)\partial_R, n_2(s)\partial_R, \partial_{X_3}) \quad \text{on upper and lower faces } (0,\infty)\times\{\pm 1\}$$

For each fixed $s \in \partial\omega$, there exists a unique exponentially decreasing three-component vector $\varphi^1(R, X_3) = \varphi^1(s; R, X_3)$ and two real numbers $\gamma^{\mathrm{b}} = \gamma^{\mathrm{b}}(s)$ and $\gamma'^{\mathrm{b}} = \gamma'^{\mathrm{b}}(s)$ such that the mixed boundary value problem in the half-strip

$$\begin{cases} \mathscr{B}(s)\psi = 0 & \text{in} \quad (0,\infty)\times(-1,1) \\ \mathscr{G}(s)\psi = 0 & \text{on} \quad (0,\infty)\times\{\pm 1\} \\ \psi = -(0, 0, \dfrac{X_3^2}{2} - \dfrac{1}{6})^{\mathrm{T}} & \text{on} \quad \{0\}\times(-1,1) \end{cases}$$

has a solution of the form (when written in normal-, tangential-to-$\partial\omega$ and vertical local components)

$$\psi = \varphi^1 + \gamma^{\mathrm{b}}\begin{pmatrix} -X_3 \\ 0 \\ R \end{pmatrix} + \gamma'^{\mathrm{b}}\begin{pmatrix} 0 \\ 0 \\ 1 \end{pmatrix}$$

Then the first boundary layer operator $\zeta \mapsto \Phi^1\zeta$ is defined by

$$(\Phi^1\zeta)(s,R,X_3) = \left.\frac{(C_{13}\partial_1^2 + C_{23}\partial_2^2)\zeta}{C_{33}}\right|_{\partial\omega}(s)\varphi^1(s;R,X_3)$$

and the boundary conditions on ζ_1 are obtained by requiring that the Dirichlet trace of components (A1) and (A2) of ansatz is a $\mathcal{O}(\varepsilon^2)$ and $\mathcal{O}(\varepsilon^3)$, respectively:

$$\zeta_1 = 0, \quad \partial_r\zeta_1 = \left.\frac{(C_{13}\partial_1^2 + C_{23}\partial_2^2)\zeta_0}{C_{33}}\right|_{\partial\omega}(s)\gamma^{\mathrm{b}}(s) \quad \text{on} \quad \partial\omega \tag{A5}$$

These boundary conditions have to be combined with the second equation arising from (A3):

$$L^{\mathrm{KL}}\zeta_1 = \Lambda_0\zeta_1 + \Lambda_1\zeta_0 \tag{A6}$$

A.3. Solution of the first two eigen-problems for the generator

The first eigen-problem is (A4). Its solutions are obviously the eigen-pairs (ζ_0, Λ_0) of the fourth-order operator L^{KL} with Dirichlet conditions. Let us fix such a Λ_0 and let $\mathscr{E}$ be the corresponding eigen-space.

The solution of the next eigen-problem (A5), (A6) is subject to *compatibility conditions* since $L^{\mathrm{KL}} - \Lambda_0$ is not invertible. The Fredholm alternative can be formulated by integrating by parts Equation (A6) against any element $\zeta_0' \in \mathscr{E}$, that is

$$0 = \int\!\!\int_\omega L^{\mathrm{KL}}\zeta_1\zeta_0' - \Lambda_0\zeta_1\zeta_0' - \Lambda_1\zeta_0\zeta_0' \,\mathrm{d}x_1\mathrm{d}x_2 \tag{A7}$$

where we integrate by parts four times the term $\iint L^{\mathrm{KL}}\zeta_1\zeta_0'$. Since ζ_0' belongs to $H_0^2(\omega)$ and ζ_1 to $H_0^1(\omega)$, we are left with the only term $-\int_{\partial\omega}\partial_r\zeta_1 P'\zeta_0'$, where P' is the second-order operator[§]

$$P'(s;\partial_1,\partial_2) = \tfrac{1}{3}(n_1^2\widetilde{C}_{11}\partial_1^2 + n_2^2\widetilde{C}_{22}\partial_2^2 + 2(\widetilde{C}_{12} + 2\widetilde{C}_{66})n_1n_2\partial_1\partial_2)$$

Further, we know from (A5) that

$$\partial_r\zeta_1 = \gamma^{\mathrm{b}}(s)P(\partial_1,\partial_2) = \frac{C_{13}\partial_1^2 + C_{23}\partial_2^2}{C_{33}}\zeta_0$$

Then from (A7), together with the equations $L^{\mathrm{KL}}\zeta_0' = \Lambda_0\zeta_0'$ we deduce

$$0 = \int_{\partial\omega}\gamma^{\mathrm{b}}(s)P\zeta_0\,P'\zeta_0'\,\mathrm{d}s + \int\!\!\int_\omega \Lambda_1\zeta_0\zeta_0'\,\mathrm{d}x_1\mathrm{d}x_2 \tag{A8}$$

[§]We have used the relations $\partial_\alpha\zeta_1 = n_\alpha\partial_r\zeta_1$ valid on $\partial\omega$ for $\alpha = 1,2$, since $\partial_s\zeta_1 = 0$ on $\partial\omega$.

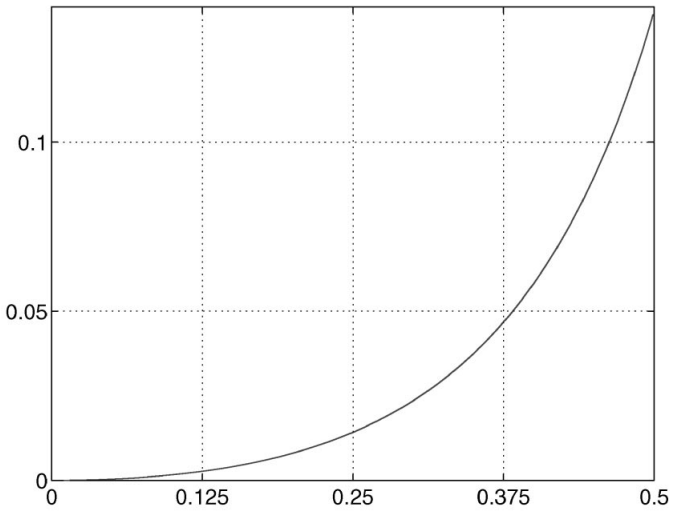

Figure 18. The 'constant' $c^{\mathrm{b}}(\nu)$ as a function of ν for isotropic materials.

Using that for any element $\zeta \in H_0^2(\omega)$, there holds $\partial_\alpha \partial_\beta \zeta = n_\alpha n_\beta \partial_r^2$ on $\partial\omega$, and setting

$$c^{\mathrm{b}}([C];s) := -\gamma^{\mathrm{b}}(s)\frac{n_1^4\widetilde{C}_{11} + n_2^4\widetilde{C}_{22} + 2(\widetilde{C}_{12} + 2\widetilde{C}_{66})n_1^2n_2^2}{3}\frac{n_1^2C_{13} + n_2^2C_{23}}{C_{33}} \tag{A9}$$

we obtain that, to be associated with a pair (ζ_1, Λ_1), an element $\zeta_0 \in \mathscr{E}$ has to satisfy for all $\zeta_0' \in \mathscr{E}$

$$\int_{\partial\omega} c^{\mathrm{b}}([C];s)\partial_r^2\zeta_0\,\partial_r^2\zeta_0'\,\mathrm{d}\,s = \Lambda_1 \int\!\!\int_\omega \zeta_0\zeta_0'\,\mathrm{d}\,x_1\,\mathrm{d}\,x_2 \tag{A10}$$

which means that (ζ_0, Λ_1) is an eigen-pair of the symmetric eigen-problem (A10). The positivity of the function $-\gamma^{\mathrm{b}}(s)$ can be proved by the same arguments as in [9, Section 6.2]. The positivity of the other functions in (A9) constituting c^{b} results from the positivity of the material matrix $[C]$.

Noting that for $\zeta \in H_0^2(\omega)$, there holds $\partial_r^2\zeta = \Delta\zeta$ on $\partial\omega$, we obtain formula (12) in the case when Λ_0 is a simple eigenvalue. For isotropic materials, the 'constant' $c^{\mathrm{b}}(\nu)$ introduced in (8) is plotted for $\nu \in [0, 0.5)$ in Figure 18. It resembles the one plotted in Reference [3].

For non-isotropic materials, $c^{\mathrm{b}}([C];s)$ also depends on s via the orientation of the material fibres with respect to the boundary at point s. Considering $(n_1, n_2) = (\cos\theta, \sin\theta)$, we may consider $c^{\mathrm{b}}([C])$ as a function $c^{\mathrm{b}}([C];\theta)$ of θ. For both orthotropic and strongly orthotropic materials used in our computations, the function $\theta/\pi \mapsto c^{\mathrm{b}}([C];\theta)$ is plotted for $\theta/\pi \in [0,1]$ in Figure 19. We note that c^{b} takes larger values for the orthotropic material than for isotropic materials, and still larger values for the strongly orthotropic material. The period $1/2$ is due to the symmetries of our materials.

The computations for Figures 18 and 19 are carried out with the Finite Element library Mélina [10].

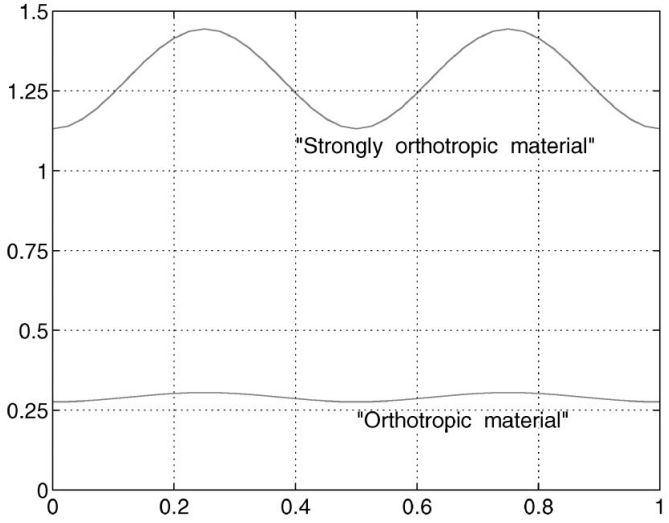

Figure 19. The function $\theta/\pi \mapsto c^{\mathrm{b}}([C];\theta)$ for both orthotropic materials.

APPENDIX B: R–M EIGEN-VALUES—ASYMPTOTICS FOR ORTHOTROPIC PLATES

In this appendix, we describe the first steps of the asymptotic analysis for the R–M eigen-pairs, solution of (20). In order to have simpler formulations of the underlying operators, introducing no essential restriction we assume

$$\widetilde{C}_{44} = \widetilde{C}_{55} = 1$$

On the other hand, we define the following 2×2 bi-dimensional elasticity system M^{KL}:

$$\boldsymbol{\beta} \mapsto M^{\mathrm{KL}}\boldsymbol{\beta} = \frac{1}{3}\begin{cases} \widetilde{C}_{11}\partial_1^2\beta_1 + \widetilde{C}_{12}\partial_1\partial_2\beta_2 + \widetilde{C}_{66}(\partial_2^2\beta_1 + \partial_1\partial_2\beta_2) \\ \widetilde{C}_{22}\partial_1^2\beta_2 + \widetilde{C}_{12}\partial_1\partial_2\beta_1 + \widetilde{C}_{66}(\partial_1^2\beta_2 + \partial_1\partial_2\beta_1) \end{cases} \tag{B1}$$

We note that the system M^{KL} has the following relation with the K–L operator L^{KL} defined in (5):

$$\operatorname{div} M^{\mathrm{KL}}\nabla = L^{\mathrm{KL}} \tag{B2}$$

Then eigen-problem (20) can be written in the form

$$\begin{cases} -\varepsilon^3 M^{\mathrm{KL}}\boldsymbol{\beta} - \varepsilon(\nabla w - \boldsymbol{\beta}) = \frac{1}{3}\varepsilon^3\widetilde{\lambda}^2\boldsymbol{\beta} \\ -\varepsilon \operatorname{div}(\nabla w - \boldsymbol{\beta}) = \varepsilon\widetilde{\lambda}^2 w \end{cases} \tag{B3}$$

with the Dirichlet boundary conditions

$$\beta_1 = \beta_2 = w = 0 \quad \text{on } \partial\omega$$

Setting $\widetilde{\lambda}^2 = \varepsilon^2 \Lambda$, we obtain that (B3) is equivalent to

$$\begin{cases} -\varepsilon^2 M^{\mathrm{KL}} \boldsymbol{\beta} - (\nabla w - \boldsymbol{\beta}) = \frac{1}{3}\varepsilon^4 \Lambda \boldsymbol{\beta} \\ -\mathrm{div}(\nabla w - \boldsymbol{\beta}) = \varepsilon^2 \Lambda w \end{cases} \tag{B4}$$

As there are only *even* powers of ε in (B4) we start with even Ansätze: for Λ,

$$\Lambda = \Lambda_0 + \varepsilon^2 \Lambda_2 + \cdots$$

and for $\boldsymbol{\beta}$ and w

$$\boldsymbol{\beta} = \boldsymbol{\beta}_0 + \varepsilon^2 \boldsymbol{\beta}_2 + \varepsilon^4 \boldsymbol{\beta}_4 + \cdots \quad \text{and} \quad w = w_0 + \varepsilon^2 w_2 + \varepsilon^4 w_4 + \cdots$$

Using these Ansätze in (B4) and identifying the powers of ε we find systems of equations on Λ_k, $\boldsymbol{\beta}_k$ and w_k, the first three ones of which are

$$\begin{cases} -(\nabla w_0 - \boldsymbol{\beta}_0) = 0 \\ -\mathrm{div}(\nabla w_0 - \boldsymbol{\beta}_0) = 0 \end{cases} \tag{B5}$$

$$\begin{cases} -M^{\mathrm{KL}} \boldsymbol{\beta}_0 - (\nabla w_2 - \boldsymbol{\beta}_2) = 0 \\ -\mathrm{div}(\nabla w_2 - \boldsymbol{\beta}_2) = \Lambda_0 w_0 \end{cases} \tag{B6}$$

$$\begin{cases} -M^{\mathrm{KL}} \boldsymbol{\beta}_2 - (\nabla w_4 - \boldsymbol{\beta}_4) = \frac{1}{3}\Lambda_0 \boldsymbol{\beta}_0 \\ -\mathrm{div}(\nabla w_4 - \boldsymbol{\beta}_4) = \Lambda_0 w_2 + \Lambda_2 w_0 \end{cases} \tag{B7}$$

Here follow all the equations satisfied by Λ_0, Λ_2, $\boldsymbol{\beta}_0$, $\boldsymbol{\beta}_2$, w_0 and w_2 so that (B5)–(B7) hold:

$$\boldsymbol{\beta}_0 = \nabla w_0 \tag{B8}$$

$$\boldsymbol{\beta}_2 = \nabla w_2 + M^{\mathrm{KL}} \nabla w_0 \tag{B9}$$

$$(L^{\mathrm{KL}} - \Lambda_0) w_0 = 0 \tag{B10}$$

$$(L^{\mathrm{KL}} - \Lambda_0) w_2 = \Lambda_2 w_0 + (\tfrac{1}{3}\Lambda_0 \Delta + \mathrm{div}\, M^{\mathrm{KL}} M^{\mathrm{KL}} \nabla) w_0 \tag{B11}$$

Equations (B8) and (B10) combined with the boundary conditions $w_0 = 0$ and $\boldsymbol{\beta}_0 = 0$ are solved by the eigen-pairs (w_0, Λ_0) of the operator L^{KL} with Dirichlet boundary conditions $w_0 = 0$ and $\partial_n w_0 = 0$ on $\partial\omega$.

As for equation (B11), for any pair of fixed traces g and h, we can find[||] (w_2, Λ_2) satisfying (B11) together with the boundary conditions $w_2 = g$ and $\partial_n w_2 = h$ on $\partial\omega$. In order to satisfy the Dirichlet conditions $\boldsymbol{\beta}_2$, w_2 are zero on $\partial\omega$, and taking (B9) into account, we may choose

$$g = 0 \quad \text{and} \quad h = -\partial_n M^{\mathrm{KL}} \nabla w_0 \tag{B12}$$

[||]If Λ_0 is a *simple eigenvalue* of L^{KL}. The case of multiple eigenvalues has to be treated like above, see Appendix A.

Then w_2 and the normal component of $\boldsymbol{\beta}_2$ are zero on $\partial\omega$. As for the tangential component of $\boldsymbol{\beta}_2$, since $\partial_s w_2 = 0$ on $\partial\omega$, its trace is equal to the tangential component χ of $M^{\mathrm{KL}}\nabla w_0$, which has no reason to be zero.

In the *isotropic case*, the trace $\varepsilon^2\chi$ of the tangential component of $\boldsymbol{\beta}_0 + \varepsilon^2\boldsymbol{\beta}_2$ is compensated by the first boundary layer term in the expansion of the eigen-vector: this term has the form $\varepsilon^2(\boldsymbol{\Psi}, \varepsilon W)(s, R)$, where we recall that R is the scaled variable r/ε. Here, we simply obtain that $W = 0$, the normal component Ψ_n of $\boldsymbol{\Psi}$ is zero, and for each $s \in \partial\omega$ the tangential component $\Psi_s(s, \cdot)$ is the exponentially decreasing solution of the boundary value problem on $\mathbb{R}_+$:

$$-\widetilde{C}_{66}\partial_R^2\Psi_s + \Psi_s = 0, \quad \forall R > 0, \quad \text{and} \quad \Psi_s(s, 0) = -\chi(s) \tag{B13}$$

This fits perfectly with the loading case in References [4, 5].

In the general orthotropic case, we do not have any more this uncoupling between normal and tangential components of $\boldsymbol{\Psi}$. The first boundary layer term still has the form $\varepsilon^2(\boldsymbol{\Psi}, \varepsilon W)(s, R)$ and the triple $(\boldsymbol{\Psi}, W)(s, \cdot)$ solves the system

$$\mathscr{R}(s; \partial_R)(\boldsymbol{\Psi}, W) = 0, \quad \forall R > 0$$

where, if $R(\partial_1, \partial_2)$ denotes the system $(\boldsymbol{\beta}, w) \mapsto (-M^{\mathrm{KL}}\boldsymbol{\beta} + \boldsymbol{\beta} - \nabla w, \mathrm{div}\boldsymbol{\beta} - \Delta w)$,

$$\mathscr{R}(s; \partial_R) := R(n_1(s)\partial_R, n_2(s)\partial_R)$$

Then there exists a unique exponentially decreasing solution of the boundary value problem on $\mathbb{R}_+$:

$$\mathscr{R}(s; \partial_R)(\boldsymbol{\Psi}, W) = 0, \quad \forall R > 0, \quad \text{and} \quad \Psi_s(s, 0) = -\chi(s) \tag{B14}$$

But now, in general, Ψ_n and W are not $\equiv 0$. As the power of ε in front of W is 3, the trace of W does not disturb the trace of $w_0 + \varepsilon^2 w_2$. This means that we keep the choice of the boundary condition $g = 0$ for w_2 in (B12). But we have to modify h by setting instead of $h = -\partial_n M^{\mathrm{KL}}\nabla w_0$:

$$h = -\partial_n M^{\mathrm{KL}}\nabla w_0 - \Psi_n(s, 0)$$

Then the expansion of the R–M eigenvector starts with

$$\boldsymbol{\beta}_0 + \varepsilon^2\boldsymbol{\beta}_2 + \varepsilon^2\boldsymbol{\Psi}(s, R) + \mathscr{O}(\varepsilon^3) \quad \text{and} \quad w_0 + \varepsilon^2 w_2 + \mathscr{O}(\varepsilon^3)$$

and that of the eigenvalue with

$$\Lambda_0 + \varepsilon^2\Lambda_2 + \mathscr{O}(\varepsilon^3)$$

where Λ_2 is influenced by the boundary layer only in the non-isotropic case (when h has to be modified).

REFERENCES

1. Ciarlet PG, Kesavan S. Two-dimensional approximation of three-dimensional eigenvalue problems in plate theory. *Computer Methods in Applied Mechanics and Engineering* 1981; **26**:149–172.
2. Dauge M, Djurdjevic I, Faou E, Rössle A. Eigenmodes asymptotic in thin elastic plates. *Journal de Mathematiques Pures et Appliquees* 1999; **78**:925–964.

3. Nazarov SA, Zorin IS. Edge effect in the bending of a thin three-dimensional plate. *Prikladnaya Matematical Mekhanika* 1989; **53**(4):642–650. (English translation *Journal of Applied Mathematics & Mechanics* 1989; 500–507.
4. Arnold DN, Falk RS. The boundary layer for the Reissner–Mindlin plate model. *SIAM Journal of Mathematical Analysis* 1990; **21**(2):281–312.
5. Arnold DN, Falk RS. Asymptotic analysis of the boundary layer for the Reissner–Mindlin plate model. *SIAM Journal of Mathematical Analysis* 1996; **27**(2):486–514.
6. Dauge M, Gruais I. Asymptotics of arbitrary order for a thin elastic clamped plate. I: optimal error estimates. *Asymptotic Analysis* 1996; **13**:167–197.
7. Babuška I, d'Harcourt JM, Schwab C. Optimal shear correction factors in hierarchic plate modelling. *Mathematical Modelling and Science of Computing*. 1991; **1**:1–30.
8. Szabó B, Babuška I. *Finite Element Analysis*. Wiley: New York, 1991.
9. Dauge M, Gruais I, Rössle A. The influence of lateral boundary conditions on the asymptotics in thin elastic plates. *SIAM Journal of Mathematical Analysis* 1999/00; **31**(2):305–345 (electronic).
10. Martin D. Mélina. On line documentation: URL `http://www.maths.univ-rennes1.fr/~dmartin`.

